Bidirectional regulation of thermotaxis by glutamate transmissions in *Caenorhabditis elegans*

Noriyuki Ohnishi[1], Atsushi Kuhara[1], Fumiya Nakamura[1], Yoshifumi Okochi[1,4] and Ikue Mori[1,2,3,*]

[1]Laboratory of Molecular Neurobiology, Division of Biological Science, Department of Molecular Biology, Graduate School of Science, Nagoya University, Nagoya, Japan, [2]CREST, Japan Science and Technology Agency, Saitama, Japan and [3]Institute for Advanced Research, Nagoya University, Nagoya, Japan

In complex neural circuits of the brain, massive information is processed with neuronal communication through synaptic transmissions. It is thus fundamental to delineate information flows encoded by various kinds of transmissions. Here, we show that glutamate signals from two distinct sensory neurons bidirectionally affect the same postsynaptic interneuron, thereby producing the opposite behaviours. EAT-4/VGLUT (vesicular glutamate transporter)-dependent glutamate signals from AFD thermosensory neurons inhibit the postsynaptic AIY interneurons through activation of GLC-3/GluCl inhibitory glutamate receptor and behaviourally drive migration towards colder temperature. By contrast, EAT-4-dependent glutamate signals from AWC thermosensory neurons stimulate the AIY neurons to induce migration towards warmer temperature. Alteration of the strength of AFD and AWC signals led to significant changes of AIY activity, resulting in drastic modulation of behaviour. We thus provide an important insight on information processing, in which two glutamate transmissions encoding opposite information flows regulate neural activities to produce a large spectrum of behavioural outputs.

Introduction

Immense neural information is processed in complex neural circuits of the brain. In the course of processing, neurons communicate neural information through synaptic transmissions. To gain insight on information processing, it is fundamental to delineate how each information flow communicates in the circuits, thereby modulating behavioural outputs. Although studies in vertebrates have provided a wealth of data on the neural communication through synaptic transmissions, dissection of information flow conveyed between neurons has been hindered by difficulty of the identification of neural codes because of the complexity of the vertebrate nervous system (Di Maio, 2008).

The nematode *Caenorhabditis elegans* is well suited for the analysis of information processing in the circuits, because of its accessible genetics (Brenner, 1974), *in vivo* physiological techniques (Kerr *et al*, 2000), and the simple nervous system with entirely known synaptic connections and gap junctions (White *et al*, 1986). Of various behaviours analysed to date (de Bono and Maricq, 2005), thermotaxis is best known for its behavioural plasticity: the animals remember the ambient temperature in association with the past feeding condition, and migrate to and move isothermally around the previous experienced temperature on a temperature gradient (Hedgecock and Russell, 1975; Mori and Ohshima, 1995; Mohri *et al*, 2005). According to the neural circuit model for thermotaxis (Mori and Ohshima, 1995), temperature is sensed and remembered by AFD and AWC sensory neurons, thermal information from AFD and AWC is transmitted to AIY interneuron, and the subsequent information from AIY is transmitted to AIZ and RIA interneurons for further neural information processing (Figure 2D; Mori and Ohshima, 1995; Clark *et al*, 2006; Biron *et al*, 2008; Kuhara *et al*, 2008). Several molecular components related to temperature sensing signal transduction have been identified. In AFD neurons, three guanylyl cyclases, GCY-8, GCY-18, and GCY-23, appear to redundantly produce cGMP, and cGMP-dependent cation channel composed of TAX-2 and TAX-4 increase internal calcium concentration on reception of temperature change (Komatsu *et al*, 1996; Kimura *et al*, 2004; Inada *et al*, 2006). In AWC neurons, ODR-1 (guanylyl cyclase) produces cGMP through activation of ODR-3 (G-α), and TAX-4 (cGMP-dependent cation channel) increases internal calcium concentration on reception of temperature stimuli (Kuhara *et al*, 2008). However, it remains to be understood how neurons communicate with each other to modulate the neural activity that generates thermotactic behaviour.

EAT-4 is a *C. elegans* homologue of mammalian vesicular glutamate transporter (VGLUT) that concentrates glutamate into synaptic vesicles (Lee *et al*, 1999; Bellocchio *et al*, 2000; Takamori *et al*, 2000), and involved in chemotaxis, habituation of the tap withdrawal response, local search, and migration towards colder temperature (Rankin and Wicks, 2000; Hills *et al*, 2004; Chalasani *et al*, 2007; Clark *et al*, 2007).

*Corresponding author. Laboratory of Molecular Neurobiology, Division of Biological Science, Department of Molecular Biology, Graduate School of Science, Nagoya University, Nagoya, Aichi 464-8602, Japan. Tel.: +81 52 789 4560; Fax: +81 52 789 4558; E-mail: m46920a@nucc.cc.nagoya-u.ac.jp
[4]Present address: Laboratory of Integrative Physiology, Graduate School of Medicine, Osaka University, Osaka 565-0871, Japan

In this study, molecular, genetic, and calcium imaging analysis revealed that coordinated functions of EAT-4-dependent glutamate signals from AFD and AWC thermosensory neurons and from RIA interneurons are essential for thermotaxis. EAT-4-dependent glutamate signals from AFD inhibit AIY through activation of GLC-3/GluCl inhibitory glutamate receptor (Horoszok *et al*, 2001), whereas EAT-4-dependent glutamate signals from AWC stimulate AIY. Alteration of the strength of EAT-4-dependent AFD and AWC glutamate signals onto AIY leads to significant changes of AIY activity, which, through EAT-4-dependent glutamate signals from RIA, results in drastic modulation of thermotaxis. Our results provide an important insight on information processing, in which two glutamatergic synaptic transmissions encoding opposite information flows regulate neural activities to generate various behavioural outputs.

Results

VGLUT homologue EAT-4 is essential for thermotaxis behaviour

In our attempt to analyse thermotaxis-defective mutants through forward genetic approach, we isolated *nj2* and *nj6* mutants that exhibit abnormal migration in a radial temperature gradient (Supplementary Figure S1A and B). Both *nj2* and *nj6* mutations were mapped to the region including *eat-4* gene and did not complement with *eat-4(ky5)* loss-of-function mutation, suggesting that *nj2* and *nj6* mutations are allelic to *eat-4(ky5)* mutation. Our sequencing of *eat-4(nj2)* and *eat-4(nj6)* genomes revealed that *nj2* is associated with two missense mutations of the conserved amino acid (G16E) and the putative transmembrane domain (G355R), and that *nj6* is a missense mutation of the conserved amino acid (G494R; Supplementary Figure S1C; Ni *et al*, 1994).

Two types of thermotaxis assays were performed for *eat-4(ky5)* mutants. The individual thermotaxis assay is suitable for scoring isothermal tracking (IT) behaviour (Figure 1A and B; Gomez *et al*, 2001). Although many wild-type animals ($55 \pm 8\%$) exhibited IT behaviour in a radial thermal gradient from 17 to 25°C after cultivation at 20°C in well-fed conditions, no *eat-4(ky5)* mutants (0%) exhibited IT behaviour (Figure 1A and B). In addition, *eat-4(ky5)* mutants showed severe impairment in the population thermotaxis assay that is suitable for quantitatively assessing the migration ability towards the cultivation temperature (Figure 1C–E; Ito *et al*, 2006). After cultivation at 23, 20, or 17°C in well-fed condition, most of wild-type animals migrated up or down the linear temperature gradient (0.45°C/cm) until they reached the region nearly corresponding to the previous cultivation temperature (Figure 1C and D). However, *eat-4(ky5)* animals exhibited little tendency to migrate towards cultivation temperature and mostly dispersed in a wide area (Figure 1D). TTX indices (Figure 1C) of *eat-4(ky5)* mutants cultivated at both 23°C and 17°C (0.47 ± 0.14 at 23°C and -1.46 ± 0.08 at 17°C) differed significantly from those of wild-type animals (2.27 ± 0.19 at 23°C and -2.96 ± 0.22 at 17°C; Figure 1E). Although *eat-4(ky5)* mutants did not show locomotion defect, they dispersed less than wild-type animals in the absence of a temperature gradient (Supplementary Figure S2A and B; Ségalat *et al*, 1995), indicating the possibility that abnormal TTX indices of *eat-4(ky5)* mutants could result from other defects, such as local search defect. Nevertheless, *eat-4(ky5)* mutants dispersed more broadly from cultivation temperature than wild-type animals on a thermal gradient (Figure 1D). This tendency was also observed in the population thermotaxis assay of *eat-4(ky5)* mutants cultivated at 20°C after being placed at the higher and lower temperature positions in the gradient (Supplementary Figure S2C and D). These results suggest that *eat-4(ky5)* mutants indeed exhibit thermotaxis defect, implicating the behavioural regulation by EAT-4-dependent glutamatergic neurotransmission.

EAT-4/VGLUT is expressed in subsets of neurons, including constituents of the thermotaxis neural circuit

Previously, *eat-4::lacZ* and *eat-4::gfp* fusion genes, both containing the 2.4 kb fragment upstream of *eat-4* as a promoter, did not appear to be expressed in critical neurons for thermotaxis (Lee *et al*, 1999). The *eat-4* gene driven by this 2.4 kb promoter did not restore the normal thermotaxis in *eat-4* mutants (Supplementary Figure S3A), suggesting that the 2.4 kb promoter does not drive sufficient expression of *eat-4* gene for thermotaxis. Given that another gene resides 5.5 kb upstream of *eat-4* gene, we constructed the fusion gene containing the *eat-4* genomic fragment and the 5.5 kb upstream fragment (Figure 2A). This *full-length eat-4::gfp* fusion gene rescued the abnormal thermotaxis of *eat-4* mutants (Supplementary Figure S3A).

To identify cells expressing EAT-4, we observed the expression pattern of *full-length eat-4::gfp* in wild-type animals (Figure 2B), and also in *unc-104(e1265)* mutants defective in UNC-104/KIF1A kinesin-like motor protein, to prevent the EAT-4::GFP-caused strong fluorescence of the nerve ring (Figure 2C; Hall and Hedgecock, 1991; Otsuka *et al*, 1991). On the basis of cell-body positions and morphologies (Sulston and Horvitz, 1977; Sulston *et al*, 1983), we observed consistent expression of EAT-4::GFP in many head neurons including AFD, AWC, AIZ, and RIA, which are constituents of the thermotaxis neural circuit (Figure 2B–D; Mori and Ohshima, 1995; Kuhara *et al*, 2008).

EAT-4/VGLUT-dependent glutamatergic neurotransmissions from AFD, AWC, and RIA neurons induce multiple behavioural outputs

Consistent with the important neural function of EAT-4, expression of *eat-4* cDNA from its own promoter (5.5 kb) and in all neurons strongly rescued the IT behaviour defect of *eat-4(ky5)* mutants ($50 \pm 2\%$ and $31 \pm 2\%$, respectively, Figure 3A) and restored normal migrations to cultivation temperature ($P > 0.05$ compared with wild-type animals at every cultivation temperature; Figure 3B). To identify the neurons in which EAT-4 functions for thermotaxis, we introduced *eat-4* cDNA under the control of various cell-specific promoters into *eat-4(ky5)* mutants. Expression of EAT-4 in AFD, AWC, or AIZ did not rescue IT behaviour defect of *eat-4(ky5)* mutants (0%), whereas expression of EAT-4 in RIA weakly did ($10 \pm 2\%$; Figure 3A). Remarkably, simultaneous expression of EAT-4 in AFD and RIA rescued the defect ($39 \pm 1\%$) as strongly as the transgenic animals expressing EAT-4 from the *eat-4* promoter ($P > 0.05$; Figure 3A). The rescue efficiency of the animals expressing EAT-4 in AFD and RIA was not increased by additional expression of EAT-4 in other neurons (Figure 3A). These results suggest that EAT-4-dependent glutamate transmission from RIA to downstream
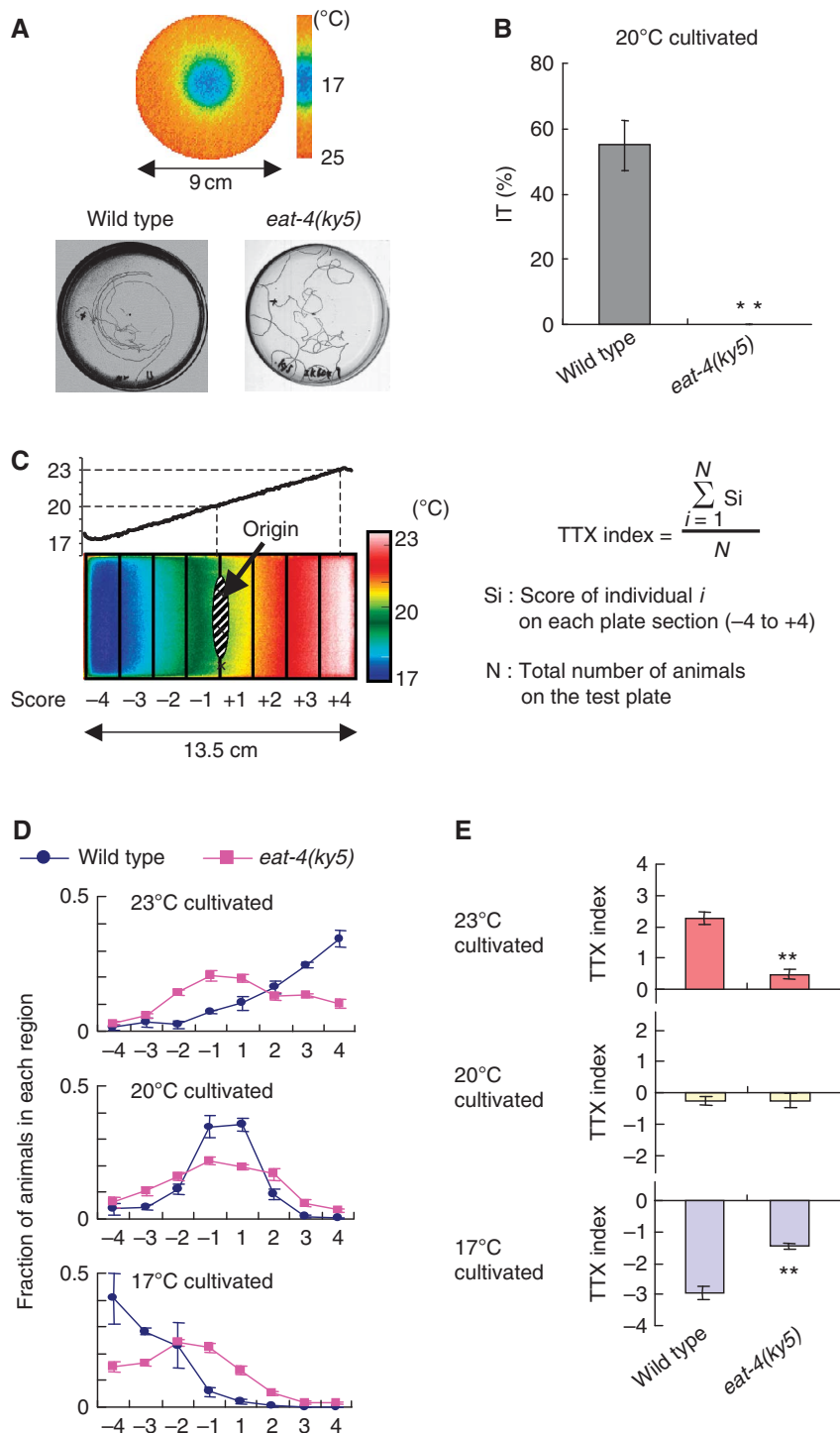
Figure 1 Thermotaxis of *eat-4(ky5)* mutants. (**A**) Individual thermotaxis assay of wild-type and *eat-4(ky5)* mutant animals. Adult animals cultivated at 20°C were individually placed on a radial thermal gradient with 17°C at the centre and 25°C at the periphery (9 cm diameter), and were allowed to move freely for 60 min (see Supplementary data for details). Most wild-type animals leave striking isothermal tracks on the assay plate, whereas *eat-4(ky5)* mutants move randomly. (**B**) Fraction of wild-type and *eat-4(ky5)* mutant animals that moved isothermally in the individual thermotaxis assay; $n = 60$ animals for both strains. Error bar indicates s.e.m. Double asterisk indicates $P < 0.01$ in ANOVA for a comparison with wild-type animals. (**C**) Procedures for population thermotaxis assay using a linear temperature gradient (Ito *et al*, 2006). About 50–200 animals cultivated at 17, 20, or 23°C were placed on the agar surface of 20°C (origin) and allowed to move freely for 60 min. The steepness of the temperature gradient was stably kept at 0.45°C/cm during the assay. The thermotactic behaviour was quantified as TTX index (see Supplementary data for details). (**D**) Distributions of wild-type and *eat-4(ky5)* mutant animals cultivated at 17, 20, or 23°C in the population thermotaxis assay. (**E**) TTX indices of wild-type and *eat-4(ky5)* mutant animals. Red bars, yellow bars, and blue bars represent TTX indices of animals cultivated at 23, 20, and 17°C, respectively; $n = 3$ or more assays. Error bar indicates s.e.m. Double asterisk indicates $P < 0.01$ in *post hoc* Tukey–Kramer tests for a comparison with wild-type animals.
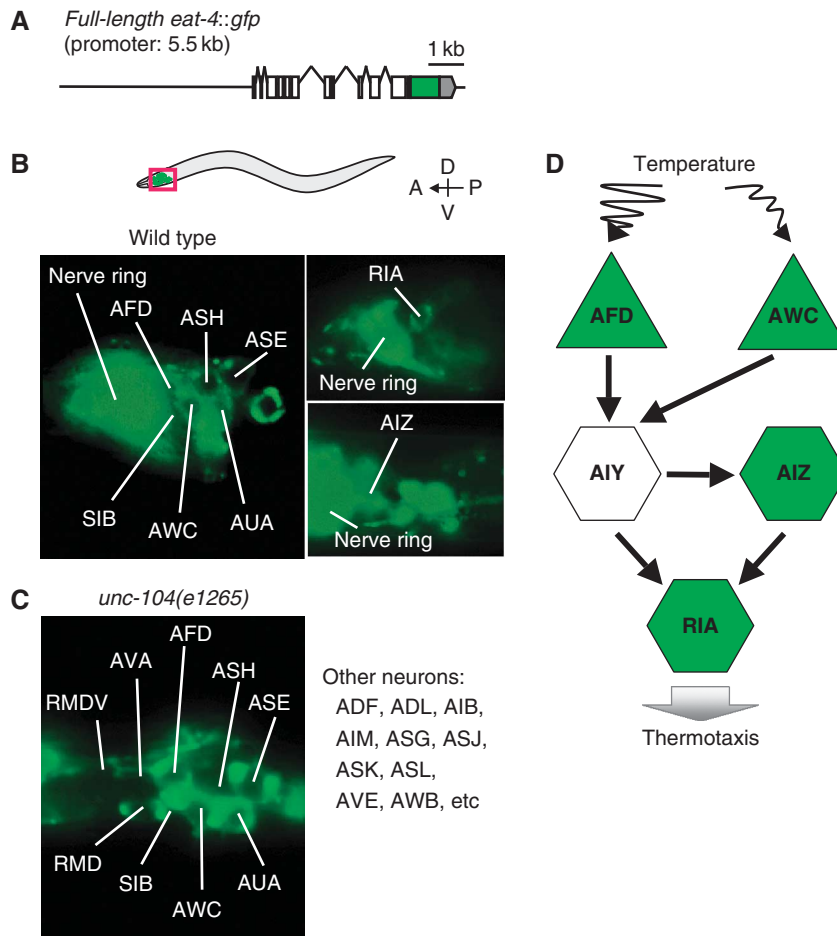
Figure 2 Expression pattern of EAT-4. (**A**) The *full-length eat-4*::*gfp* fusion gene with 5.5 kb of promoter region. (**B**,**C**) The expression of *full-length eat-4*::*gfp* in the head of wild-type animals (**B**) and of *unc-104(e1265)* mutants (**C**). Anterior is to the left and dorsal is on the top. (**B**) Fluorescence was observed in nerve ring and cell body of many neurons including AFD, AWC (left panel), RIA (top-right panel), and AIZ neurons (bottom-right panel) in wild type. (**C**) Fluorescence was not observed in the nerve ring but in the cell body of many neurons, including AFD and AWC in *unc-104(e1265)* mutants. (**D**) The proposed thermotaxis neural circuit (Mori and Ohshima, 1995; Kuhara *et al*, 2008). Temperature is sensed by AFD and AWC sensory neurons, thermal information from AFD and AWC is conveyed to AIY interneuron, and the subsequent neural information from AIY is further conveyed to AIZ and RIA interneuron. Neurons expressing the *full-length eat-4*::*gfp* are coloured green.

motor neurons is critical for conveying thermal information from AFD.

In the population thermotaxis assay, expression of EAT-4 in AIZ did not induce any changes in thermotaxis of *eat-4(ky5)* mutants as in individual thermotaxis assay (Figure 3B). Interestingly, expression of EAT-4 in AFD, AWC, or RIA induced different migration pattern from that of *eat-4(ky5)* mutants (Figure 3B), namely, the transgenic animals expressing EAT-4 in AFD migrated towards colder temperature than *eat-4(ky5)* mutants, the animals expressing EAT-4 in AWC migrated towards warmer temperature after being cultivated at 20 and 23°C, and the animals expressing EAT-4 in RIA migrated towards warmer temperature after being cultivated at 23°C (Figure 3B). Thus, EAT-4-dependent glutamate transmissions from AFD, AWC, or RIA to their postsynaptic neurons are involved in regulation of thermotaxis and each glutamate transmission induces different behavioural outputs.

Because expression of EAT-4 in RIA seems essential for thermotaxis (Figure 3A), it was difficult to detect the effect of EAT-4 only on AFD or AWC. To reconcile this problem, we introduced several doses of *AFDp*::*eat-4* cDNA and *AWCp*::*eat-4* cDNA with constant 5 ng/μl dose of *RIAp*::*eat-4*

cDNA into *eat-4(ky5)* mutants, and performed the population thermotaxis assay (Figure 3C). Simultaneous expression of EAT-4 in AFD and RIA, both in 5 ng/μl doses, enhanced migration towards colder temperature than wild-type animals after cultivation at 20 and 23°C (cryophilic movement; Figure 3C). Although tracks of these transgenic animals in the individual thermotaxis assay did not indicate cryophilic phenotype (Supplementary Figure S3B), cryophilic phenotype would not be detectable on the assay plate, in which the steepness of thermal gradient differs in different areas. Simultaneous expression of EAT-4 in AFD, AWC, and RIA with introduction of 5 ng–5 ng–5 ng/μl, 2 ng–5 ng–5 ng/μl, and 0.5 ng–5 ng–5 ng/μl of *AFDp*::*eat-4 cDNA*, *AWCp*::*eat-4 cDNA*, and *RIAp*::*eat-4 cDNA*, respectively, into *eat-4(ky5)* mutants still drove the tendency to migrate towards cold temperature, although the cryophilic response of these transgenic animals weakened as compared with the animals expressing EAT-4 in AFD and RIA (Figure 3C). By contrast, simultaneous expression of EAT-4 in AWC and RIA with 5–5 ng/μl of *AWCp*::*eat-4 cDNA* and *RIAp*::*eat-4 cDNA*, respectively, enhanced migration towards warmer temperature after cultivation at 17 and 20°C (thermophilic movement;
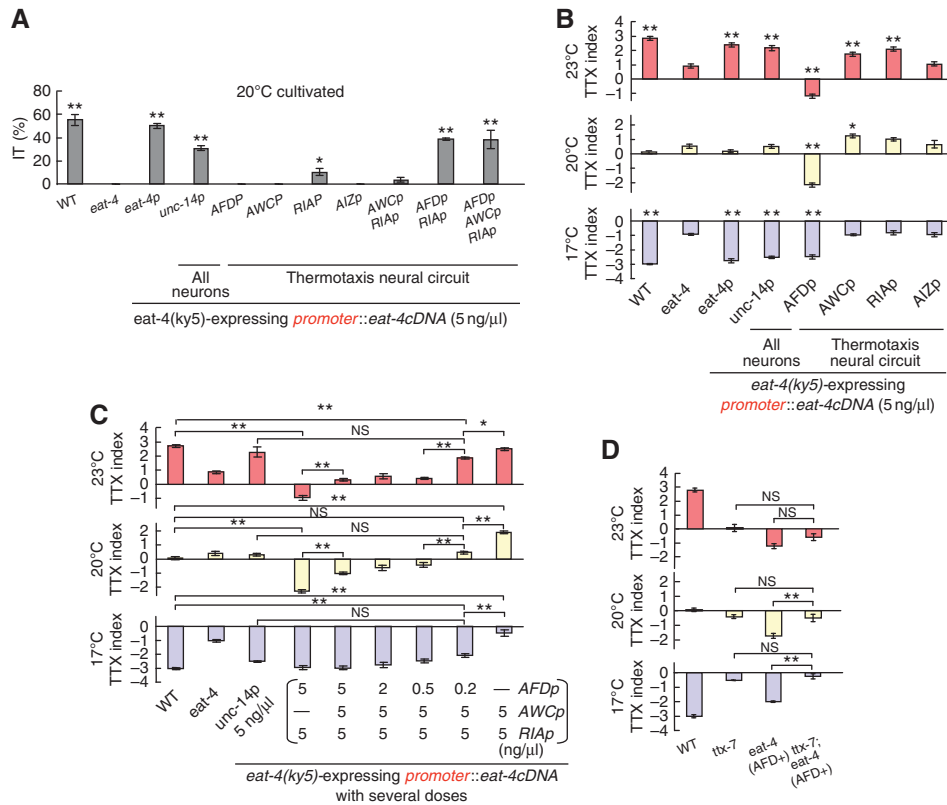
Figure 3 Cell-specific rescue experiments for thermotaxis defects of *eat-4(ky5)* mutants. (**A**) Rescue experiments for defective isothermal tracking (IT behaviour) of *eat-4(ky5)* mutants by introducing cell-specific *promoters*::*eat-4 cDNA* at 5 ng/µl; $n = 58$ or more animals. Error bar indicates s.e.m. Single and double asterisk indicate $P < 0.05$ and 0.01, respectively, in ANOVA for a comparison with *eat-4(ky5)* mutants. (**B**, **C**) Rescue experiments for defective migration to cultivation temperature of *eat-4(ky5)* mutants by introducing individual cell-specific *promoters*::*eat-4 cDNA* at 5 ng/µl (**B**) or by introducing *AFDp*::*eat-4 cDNA*, *AWCp*::*eat-4 cDNA*, and *RIAp*::*eat-4 cDNA* simultaneously at several doses (**C**); $n = 3$ or more assays. Error bars indicate s.e.m. Single asterisk, double asterisk, and NS indicate $P < 0.05$, $P < 0.01$, and $P > 0.05$ respectively, in *post hoc* Tukey–Kramer tests for a comparison with *eat-4(ky5)* mutants (**B**) and for a comparison of each genotype (**C**). (**D**) The population thermotaxis assays of *eat-4* transgenic mutants carrying genetically abnormal function in RIA. *eat-4 (AFD +)* represents the transgenic *eat-4(ky5)* mutants expressing EAT-4 in AFD; $n = \geqslant 3$ assays. Error bars indicate s.e.m. Double asterisk and NS indicate $P < 0.01$ and $P > 0.05$, respectively, in *post hoc* Tukey–Kramer tests for a comparison of each genotype.

Figure 3C). These results suggest that glutamate transmission from AFD induces cryophilic movement and that glutamate transmission from AWC induces thermophilic movement. Considering that EAT-4 in AWC was not necessary for IT behaviour (Figure 3A) and simultaneous expression of EAT-4 in AFD, AWC, and RIA induced migration towards cold temperature until the introduction dose of *AFDp*::*eat-4 cDNA* was reduced up to less than one-tenth of *AWCp*::*eat-4 cDNA* (Figure 3C), AFD-mediated glutamate transmission is likely to be more influential than AWC-mediated glutamate transmission for thermotaxis behaviour. Noticeably, simultaneous expression of EAT-4 in AFD, AWC, and RIA with 0.2 ng–5 ng–5 ng/µl of *AFDp*::*eat-4 cDNA*, *AWCp*::*eat-4 cDNA*, and *RIAp*::*eat-4 cDNA*, respectively, almost restored the normal migration to cultivation temperature and showed similar behaviour to that of *eat-4(ky5)* mutants expressing EAT-4 in all neurons (Figure 3C). These results further support that EAT-4-dependent glutamate transmission from AFD, AWC, and RIA regulates thermotaxis behaviour (Figure 3B).

RIA neurons have multiple neurotransmitter outputs

As already described in Figure 3A, EAT-4-dependent glutamate transmission from RIA is crucial for thermotaxis. Nevertheless, *eat-4* transgenic mutants expressing EAT-4 only in AFD but not in RIA (*eat-4 (AFD +)*) could migrate

to colder temperature, as opposed to *eat-4(ky5)* mutants that dispersed in broader area in the population thermotaxis assay (Figures 1D and 3B). In addition, the phenotype of *eat-4 (AFD +)* did not change with additional expression of EAT-4 in RIA (Figure 3C). These results raise two possibilities: signals from AFD flow either through RIA-independent pathway or through RIA-dependent pathway coupled with both EAT-4-dependent and -independent synaptic transmissions. To distinguish these possibilities, we examined the effect of genetically imparied RIA on *eat-4 (AFD +)* (Figure 3D). Correct localization of synapses in RIA requires TTX-7/ IMPase, and *ttx-7(nj50)* mutants showed abnormal thermotactic phenotype, similar to that of wild-type animals in which RIA was ablated (Tanizawa *et al*, 2006). Thermotactic defect of *ttx-7(nj50)* mutants completely masked the defect of *eat-4 (AFD +)* (Figure 3D), suggesting the essential role of RIA-dependent pathway involving both EAT-4-dependent and -independent transmissions.

Glutamatergic neurotransmissions from AFD and AWC neurons oppositely modulate activity of postsynaptic neuron AIY

To analyse molecular physiology of the EAT-4-dependent glutamate transmission for thermotaxis, we conducted calcium imaging of AIY, which is postsynaptic to both AFD and
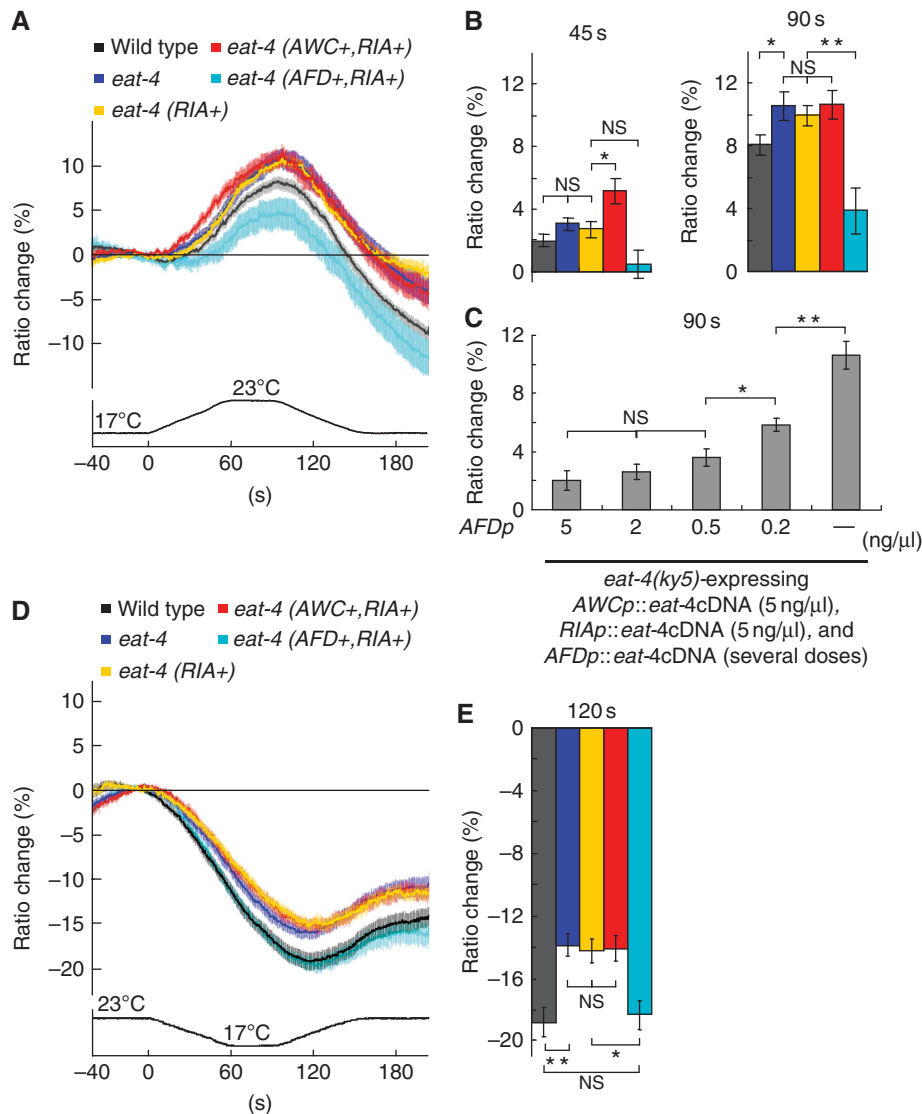
Figure 4 *In vivo* calcium imaging of AIY according to temperature change in *eat-4(ky5)* mutants and the *eat-4(ky5)* transgenic animals. (**A**) The intracellular calcium concentration change was measured as the YFP/CFP fluorescence change (ratio change) of cameleon (yc3.6). *eat-4 (AWC + , RIA +)*, *eat-4 (AFD + , RIA +)*, and *eat-4 (RIA +)* represent the transgenic *eat-4(ky5)* mutants expressing EAT-4 in AWC and RIA but not in AFD, in AFD and RIA but not in AWC, and in RIA but not in AFD and AWC, respectively (top). Response curves represent the average of ratio change according to temperature change. Temperature change along time is shown at the bottom of the response curve. 0 s is the time starting temperature change from 17 to 23°C (bottom). (**B**) The average of ratio changes to temperature stimuli at 45 s (left) and at 90 s (right), regarding the results shown in Figure 4A. The colour of bars in the graphs corresponds to the colour of response curves described in Figure 4A. (**C**) The average of ratio changes of *eat-4(ky5)* expressing EAT-4 in AFD, AWC, and RIA simultaneously by introducing several doses of *AFDp::eat-4 cDNA* with 5 ng/μl of *AWCp::eat-4 cDNA* and *RIAp::eat-4 cDNA* at 90 s. (**D**) Ratio change of yc3.6 in AIY in response to temperature change from 23 to 17°C. (**E**) The average of ratio changes to temperature stimuli at 120 s for the results shown in **D**; (**A–E**) $n = 18$ or more animals. Error bar indicates s.e.m. Single asterisk, double asterisk, and NS indicate $P < 0.05$, $P < 0.01$, and $P > 0.05$, respectively, in Steel–Dwass tests for a comparison of each genotype.

AWC (Figure 2D). We monitored temperature stimulus-evoked calcium concentration changes of AIY using cameleon, a genetically encoded calcium indicator (Miyawaki *et al*, 1997; Nagai *et al*, 2004). We verified that expression of cameleon (yc3.60) in AIY itself did not affect thermotaxis (Supplementary Figure S3C). Calcium imaging was carried out in animals cultivated at 20°C (Figure 4). Consistent with our previous results, the calcium concentration in AIY of wild-type animals increased with warming and decreased with cooling (Figure 4A and D; Kuhara *et al*, 2008). The fluorescence resonance energy transfer (FRET) ratios did not return to baseline, which might be caused by faster degradation of YFP fluorescence than CFP fluores-

cence in yc3.60 (Figure 4A and D; Supplementary Figure S4A and B). On warming, FRET ratios in AIY of *eat-4(ky5)* mutants increased more than that of wild-type animals ($11 \pm 1\%$ for *eat-4(ky5)* mutants and $8 \pm 0.6\%$ for wild-type animals at 90 s after starting temperature change; Figure 4A and B). Thus, AIY of *eat-4(ky5)* mutants appear to be hyper-responsive to warming, suggesting that EAT-4-dependent glutamate transmission is involved in the thermal response of AIY.

Previous reports showed that activation of AIY mediates movement towards warmer temperature (Mori and Ohshima, 1995; Hobert *et al*, 1997; Kuhara *et al*, 2008), implicating the correlation between the activity of AIY and behavioural

output. We then hypothesized that glutamate transmissions from AFD and AWC have opposite effects on the activity of AIY neurons, consistent with the opposite effect of AFD and AWC on behavioural outputs. To test this hypothesis, we monitored the activity of AIY on warming in transgenic *eat-4(ky5)* animals expressing EAT-4 in either AFD or AWC (Figure 4A and B) by calcium imaging. As EAT-4 in RIA is essential for thermotaxis (Figure 3A), we also expressed EAT-4 in RIA of transgenic animals (Figure 4A and B). The FRET ratio changes in AIY of *eat-4(ky5)* mutants expressing EAT-4 in RIA (*eat-4 (RIA +)*) were larger than those of wild-type animals and similar to those of *eat-4(ky5)* mutants (*eat-4*; $10 \pm 0.6\%$ at 90 s; Figure 4A and B), suggesting that expression of EAT-4 in RIA has almost no effect on the AIY activity. The larger increment in the FRET ratio of *eat-4 (RIA +)* on warming was consistent with our behavioural results showing that *eat-4 (RIA +)* exhibited the tendency to migrate towards warmer temperature after cultivation at 23°C, whereas the similar larger increment in the FRET ratio of *eat-4(ky5)* mutants was not coincided with their behavioural output (Figure 3B). Thus, EAT-4 in RIA is likely to be important for coupling AIY activity and behavioural output. Additional expression of EAT-4 in AFD of *eat-4(ky5)* mutants (*eat-4 (AFD + , RIA +)*) induced significantly smaller change of FRET ratios in AIY ($3.9 \pm 1.5\%$ at 90 s) as compared with *eat-4(ky5)* mutants and wild-type animals (Figure 4A and B). Notably, smaller changes in FRET ratio observed in *eat-4 (AFD + , RIA +)* were similarly observed in *eat-4(ky5)* mutants expressing EAT-4 only in AFD (*eat-4 (AFD +)*), which argues against any feedback pathway to AIY through RIA (Supplementary Figure S4C and D). Expression of EAT-4 in AWC and RIA (*eat-4 (AWC + , RIA +)*) caused not only the larger change, such as *eat-4(ky5)* mutants (*eat-4*; $10.6 \pm 1\%$ at 90 s), but also faster change of FRET ratios in AIY ($5.1 \pm 0.7\%$ at 45 s; Figure 4A and B). Our results on calcium imaging of AIY in animals cultivated at 20°C, therefore, closely correlated with behavioural data shown in Figure 3C. We also conducted calcium imaging of AIY in wild-type animals and *eat-4(ky5)* transgenic animals cultivated at both 17°C and 23°C, and found that correlation between calcium imaging of AIY and thermotaxis behaviour was held in every cultivation temperature (Supplementary Figure S5). The data on calcium imaging suggest that glutamate transmissions from AFD or from AWC inhibit or stimulate AIY, respectively.

To verify the effect of glutamate signals on the response of AIY, we also conducted calcium imaging of AIY on cooling (Figure 4D and E). On cooling, FRET ratios in AIY of *eat-4(ky5)* mutants did not decrease as much as those of wild-type animals ($-14 \pm 0.7\%$ for *eat-4(ky5)* mutants and $-19 \pm 1.0\%$ for wild-type animals at 120 s; Figure 4D and E). Consistent with the results on warming (Figure 4A and B), this result likely represents hyperactive state of AIY in *eat-4(ky5)* mutants (Figure 4D and E). The FRET ratios in AIY of *eat-4 (RIA +)* and *eat-4 (AWC + , RIA +)* showed a similar change to those of *eat-4(ky5)* mutants ($-14 \pm 0.8\%$ for *eat-4 (RIA +)* and for *eat-4 (AWC + , RIA +)* at 120 s; Figure 4D and E), implicating no effects of glutamate signals from AWC and RIA on the response of AIY to cooling. By contrast, the FRET ratios in AIY of *eat-4 (AFD + , RIA +)* decreased to the similar level to those of wild-type animals ($-18 \pm 0.9\%$ for *eat-4 (AFD + , RIA +)* at 120 s; Figure 4D and E), suggesting that inhibition through glutamate transmission from AFD

regulates the response of AIY to cooling. Altogether, these results demonstrate that glutamate transmission from AFD inhibits AIY activity in response to both warming and cooling, and glutamate transmission from AWC stimulates AIY activity in response to only warming, thereby implying that AFD-mediated glutamate transmission more effectively contributes to thermotaxis behaviour than AWC-mediated glutamate transmission.

To elucidate whether various behavioural outputs shown in Figure 3C are caused by modulation of AIY activity through EAT-4-dependent glutamate transmission from AFD and AWC, we investigated dose dependency of AIY activity in transgenic *eat-4(ky5)* mutants expressing relative different doses of EAT-4 in AFD, AWC, and RIA with calcium imaging on warming (Figure 4C). Intriguingly, FRET ratios showed similar small changes when introducing 5, 2, or 0.5 ng of *AFDp::eat-4 cDNA* to the *eat-4* mutants, whereas FRET ratios dramatically increased when introducing 0.2 or 0 ng of *AFDp::eat-4 cDNA* (Figure 4C), which is consistent with the results of cell-specific rescue experiments (Figure 3C). These results also demonstrated that modulation of the AIY activity by opposite glutamate signals from AFD and AWC induces drastic changes in behavioural output.

GluCl homologue GLC-3 inhibits the activity of AIY interneurons in thermotaxis

Our analysis of EAT-4/VGLUT suggested that glutamate receptors receive EAT-4-dependent glutamate signals in AIY. Four classes of glutamate receptors are predicted in *C. elegans*; AMPA (α-amino-3-hydroxy-5-methyl-4-isoxazolepropionic acid)-type glutamate-gated cation channels encoded by eight *glr* genes, NMDA (*N*-methyl-D-aspartic acid)-type glutamate-gated cation channels encoded by two *nmr* genes, glutamate-gated chloride channels (GluCl) encoded by four *glc* genes and two *avr* genes, and metabotropic G-protein-coupled glutamate receptors (mGluR) encoded by three *mgl* genes (Brockie and Maricq, 2003; Yates *et al*, 2003; Dillon *et al*, 2006). Of those, MGL-1/mGluR and GLC-3/GluCl were found to be expressed in AIY (Horoszok *et al*, 2001; Wenick and Hobert, 2004), implicating that either MGL-1 or GLC-3 is required for thermotaxis as a glutamate receptor in AIY. Although *mgl-1(tm1811)* mutants migrated to their cultivation temperature normally, *glc-3(ok321)* mutants showed migration to warmer temperature than the cultivation temperature (Figure 5A). This thermotaxis defect was fully rescued by expressing GLC-3 in AIY but not in any other neurons (Figure 5A), suggesting that GLC-3/GluCl acts as a glutamate receptor in AIY for thermotaxis.

Given that the activation of AIY mediates movement towards warmer temperature (Mori and Ohshima, 1995; Hobert *et al*, 1997; Kuhara *et al*, 2008) and GluCls mediate inhibitory neurotransmission (Dent *et al*, 1997), GLC-3/GluCl presumably regulates thermotaxis through inhibition of the AIY activity. Consistent with this possibility, FRET ratios in AIY of *glc-3(ok321)* mutants changed more than those of wild-type animals ($10 \pm 0.5\%$ for *glc-3(ok321)* mutants and $6.6 \pm 0.6\%$ for wild-type animals at 90 s; Figure 5B and C), implicating the hyper-responsiveness of AIY in *glc-3(ok321)* mutants. The increased change of FRET ratios was rescued by expressing GLC-3 in AIY ($6.2 \pm 0.4\%$ at 90 s; Figure 5B and C), suggesting that GLC-3 cell autonomously inhibits the activity of AIY.
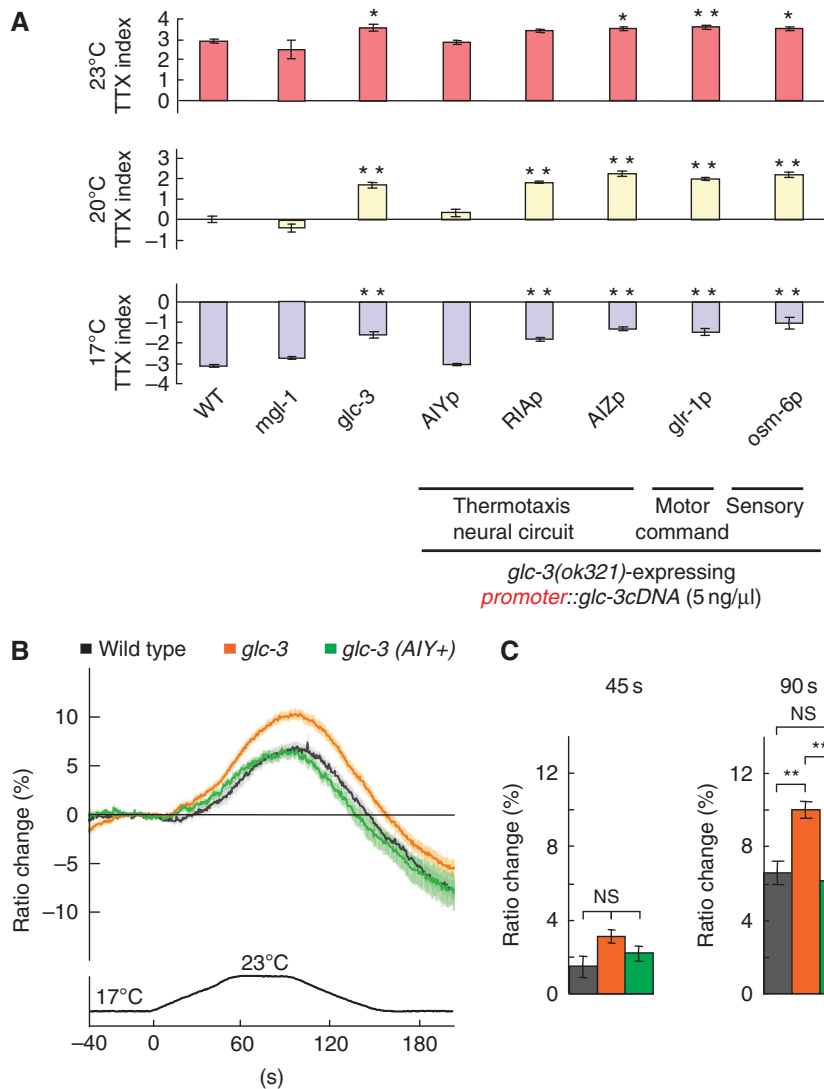
Figure 5 Cell-autonomous function of GLC-3 in thermotaxis. (**A**) The population thermotaxis assays of *mgl-1* and *glc-3* mutants, and cell-specific rescue experiments for *glc-3* mutants; $n = 3$ or more assays. Error bar indicates s.e.m. Single and double asterisk indicate $P < 0.05$ and 0.01, respectively, in *post hoc* Tukey–Kramer tests for a comparison with wild-type animals. (**B**, **C**) *In vivo* calcium imaging of AIY in *glc-3(ok321)* mutants and the *glc-3(ok321)* transgenic animals. (**B**) Ratio change of yc3.6 in AIY according to temperature change. *glc-3 (AIY +)* represents the transgenic *glc-3(ok321)* mutants expressing GCL-3 in AIY. (**C**) The average of ratio changes to temperature stimuli at 45 s (left) and at 90 s (right) regarding the results shown in **B**; (**B**, **C**) $n = 24$ or more animals. Error bar indicates s.e.m. Double asterisk and NS indicates $P < 0.01$ and $P > 0.05$, respectively, in Steel–Dwass tests for a comparison with wild-type animals.

GLC-3/GluCl receives glutamatergic signals from AFD thermosensory neurons

We addressed whether GLC-3/GluCl in AIY receives EAT-4-dependent glutamate signals from AFD or AWC. Thermosensory signal transduction in AFD is thought to be mediated by the change in intracellular concentration of cGMP through GCY-23, GCY-8, and GCY-18 guanylyl cyclases (Inada *et al*, 2006), and *gcy-23(nj37) gcy-8(oy44) gcy-18(nj38)* triple mutants showed abnormal thermotactic phenotype similar to that of AFD-ablated wild-type animals (Inada *et al*, 2006; Kuhara *et al*, 2008). *gcy-23 gcy-8 gcy-18; glc-3* quadruple mutants showed thermotactic abnormality quite similar to that of *gcy-23 gcy-8 gcy-18* triple mutants, suggesting that the abolishment of thermosensory signalling in AFD entirely suppressed the *glc-3(ok321)* mutation (Figure 6A). In addition, thermotactic defect of the *eat-4* mutants expressing EAT-4 in AWC and RIA, but not in AFD (*eat-4 (AWC + , RIA +)*), completely masked the defect of

glc-3 mutants (Figure 6A). These results suggest that GLC-3 glutamate receptors in AIY receive EAT-4-mediated glutamate signals from AFD.

Recently, ODR-3 G-α-dependent heterotrimeric G-protein-coupled signalling was found to mediate thermosensory signal transduction in AWC, and EAT-16 RGS (regulator of G-protein signalling) suppressed the G-protein-coupled signalling in AWC (Kuhara *et al*, 2008). *odr-3(n1605)* and *eat-16(nj8)* mutants migrated towards warmer and colder temperatures than the cultivation temperature, respectively (Figure 7A; Kuhara *et al*, 2008). *glc-3 odr-3* double mutants migrated to much warmer temperature than both *glc-3* and *odr-3* single mutants after cultivation at 17 and 20°C, implicating the additive effect of *odr-3* and *glc-3* mutation (Figure 7A). Similarly, thermotactic defect of *eat-16(nj8)* mutants and the *eat-4(ky5)* mutants expressing EAT-4 in AFD and RIA (*eat-4 (AFD + , RIA +)*) influenced additively on the defect of *glc-3* mutants (Figure 7A), implicating GLC-3
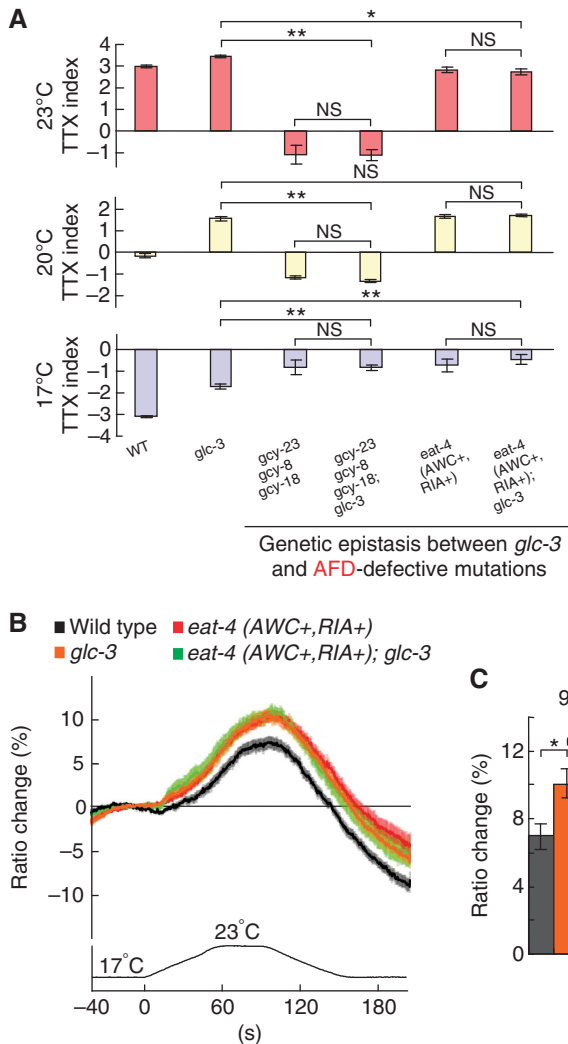
Figure 6 Effect of AFD defect on *glc-3(ok321)* mutants. (**A**) The population thermotaxis assays of AFD-defective mutants and *glc-3* mutants in the background of abnormal neural signalling in AFD; $n = 3$ or more assays. Error bar indicates s.e.m. Single asterisk, double asterisk, and NS indicate $P < 0.05$, $P < 0.01$, and $P > 0.05$, respectively, in *post hoc* Tukey–Kramer tests for a comparison of each genotype. (**B**, **C**) *In vivo* calcium imaging of AIY in *eat-4* (AWC+, RIA+); *glc-3* and in each single mutant. (**B**) Ratio change of yc3.6 in AIY according to temperature change. (**C**) The average of ratio changes to temperature stimuli at 90 s regarding the results shown in Figure 6B; (**B**, **C**) $n = 22$ or more animals. Error bar indicates s.e.m. Single asterisk and NS indicate $P < 0.05$ and $P > 0.05$, respectively, in Steel–Dwass tests for a comparison of each genotype.

independent glutamate transmission from AWC. Our genetic analyses suggest that GLC-3/GluCl is required for reception of EAT-4-dependent glutamate signals from AFD.

Using calcium imaging, we clarified whether EAT-4-dependent glutamate transmission from AFD is mediated by GLC-3 in AIY (Figures 6B, C and 7B, C). FRET ratios in AIY of the double mutants (*eat-4* (AWC+, RIA+); *glc-3*) constructed from the *eat-4* mutants expressing EAT-4 in AWC and RIA (*eat-4* (AWC+, RIA+)) and from *glc-3* mutants showed a change larger than those of wild-type animals ($9.8 \pm 0.8\%$ for double mutants and $7 \pm 0.7\%$ for wild-type animals at 90 s) and similar to those of both single mutants ($10 \pm 0.6\%$ for transgenic *eat-4* mutants and $10 \pm 0.8\%$ for *glc-3* mutants at

90 s; Figure 6B and C), thereby demonstrating the same hyper-responsiveness of double mutants as both single mutants. By contrast, FRET ratios in AIY of the double mutants (*eat-4* (AFD+, RIA+); *glc-3*) constructed from the *eat-4* mutants expressing EAT-4 in AFD and RIA (*eat-4* (AFD+, RIA+)) and from *glc-3* mutants showed the change in between those in both single mutants ($7.6 \pm 0.4\%$ for double mutants, $3.3 \pm 0.9\%$ for transgenic *eat-4* mutants, and $10 \pm 0.8\%$ for *glc-3* mutants at 90 s), but similar to those of wild-type animals (Figure 7B and C). These physiological results are consistent with the results obtained by genetic analysis, further supporting the molecular model that GLC-3 inhibits AIY on receiving EAT-4-dependent glutamate signals from AFD.

Discussion

EAT-4/VGLUT-dependent glutamatergic neurotransmission in the thermotaxis neural circuit

In the current model for temperature sensing, thermal stimuli are transduced in AFD through three functionally redundant guanylyl cyclases and cGMP-gated channels (Komatsu *et al*, 1996; Inada *et al*, 2006) and in AWC through heterotrimeric G-protein signalling and cGMP-gated channels (Kuhara *et al*, 2008). In this study, our results suggest a model for signalling pathways downstream of temperature sensing (Figure 7D). After temperature sensing in AFD and AWC sensory neurons, thermosensory information is transmitted to postsynaptic interneuron AIY through EAT-4/VGLUT-dependent glutamatergic neurotransmission. EAT-4-dependent glutamate signals from AFD inhibit AIY through activation of inhibitory glutamate receptor GLC-3/GluCl, thereby inducing migration towards colder temperature. By contrast, EAT-4-dependent glutamate signals from AWC stimulate AIY to induce migration towards warmer temperature. Hence, we demonstrated that the bidirectional regulation of AIY through EAT-4-dependent glutamate transmissions from AFD and AWC is essential for terminal behavioural phenotypes.

Previous reports showed that AFD and AWC differ in contribution for thermotaxis; AFD-ablated animals exhibited severe defect (Mori and Ohshima, 1995; Kuhara *et al*, 2008), whereas AWC-ablated animals exhibited slight defect in thermotaxis (Biron *et al*, 2008; Kuhara *et al*, 2008). These results suggested that thermotaxis is regulated by the orchestrated information in major thermosensory neuron AFD and supportive thermosensory neuron AWC. Consistent with these previous results, our behavioural and calcium imaging results demonstrated that contributions of inhibitory glutamate signals from AFD and excitatory glutamate signals from AWC are not equivalent. For IT behaviour, EAT-4-dependent glutamate transmission from AFD was indispensable, while that from AWC was not necessary (Figure 3A). In addition, transgenic *eat-4* mutants expressing EAT-4 in AFD, AWC, and RIA showed strong tendency to migrate towards colder temperature, except for the case in which the introduction dose of *AFDp::eat-4* cDNA to the *eat-4* mutants was reduced to less than one-tenth of *AWCp::eat-4* cDNA (Figure 3C). Further, glutamate transmission from AFD inhibits AIY activity in response to both warming and cooling and that from AWC stimulates AIY activity in response to only warming (Figure 4), suggesting that the contribution of inhibitory
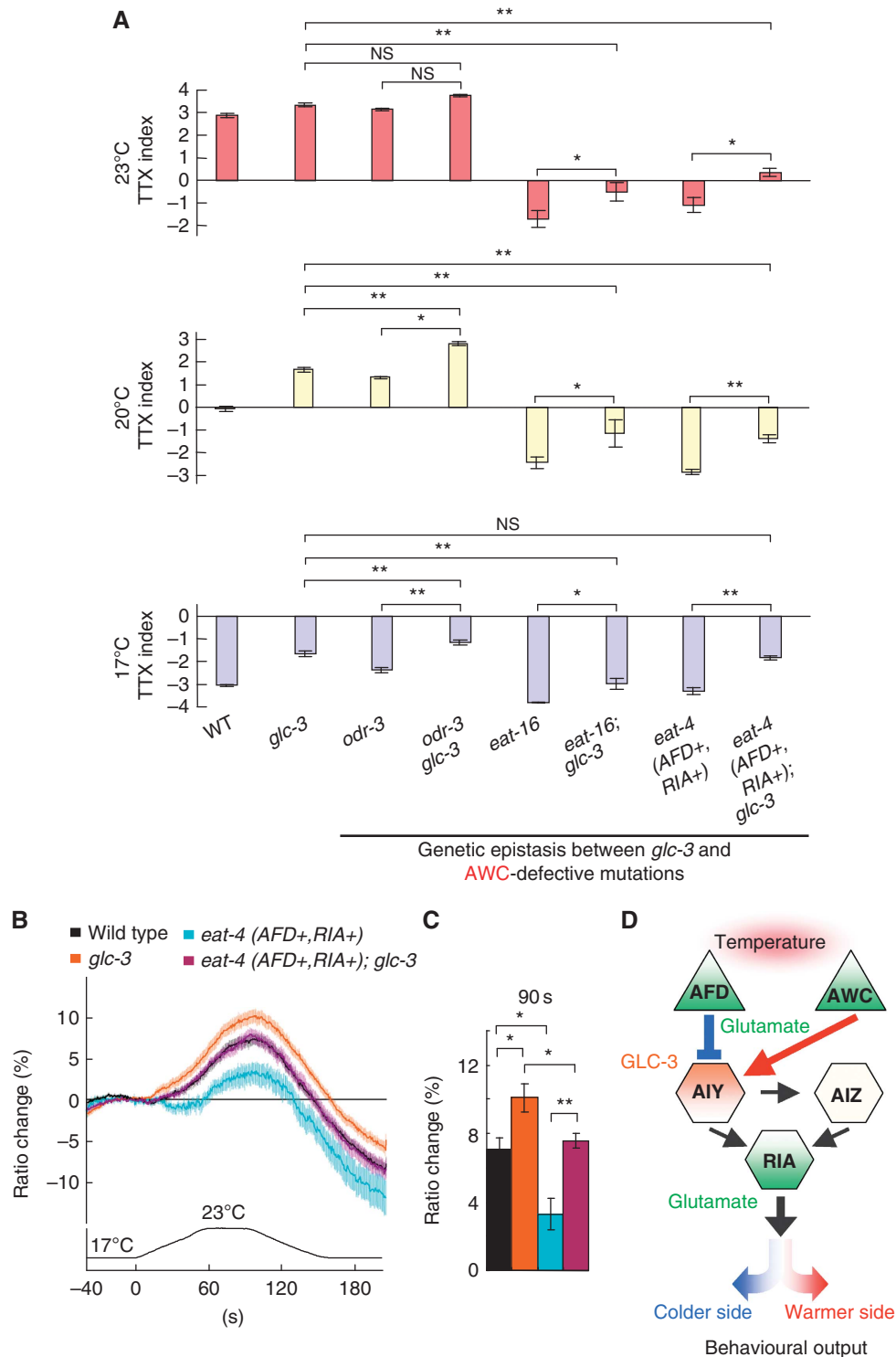
Figure 7 Effect of AWC defect on *glc-3(ok321)* mutants. (**A**) The population thermotaxis assays of AWC-defective mutants and *glc-3* mutants in the background of abnormal neural signalling in AWC; *n* = 3 or more assays. Error bar indicates s.e.m. Single asterisk, double asterisk, and NS indicate *P* < 0.05, *P* < 0.01, and *P* > 0.05, respectively, in *post hoc* Tukey–Kramer tests for a comparison of each genotype. (**B**, **C**) *In vivo* calcium imaging of AIY in *eat-4 (AFD +, RIA +); glc-3* and in each single mutant. (**B**) Ratio change of yc3.6 in AIY according to temperature change. (**C**) The average of ratio changes to temperature stimuli at 90 s regarding the results shown in **B**; (**B**, **C**) *n* = 22 or more animals. Error bar indicates s.e.m. Single and double asterisk indicate *P* < 0.05 and 0.01, respectively, in Steel–Dwass tests for a comparison of each genotype. (**D**) A model for glutamatergic neurotransmission in the thermotaxis neural circuit. AFD, AWC, and RIA release glutamate in EAT-4-dependent manner (green). GLC-3 acts in AIY (orange). EAT-4-dependent glutamate signals from AFD inhibit the activity of AIY through activation of GLC-3 inhibitory glutamate receptors, and induce eventual migration to colder side (blue). By contrast, EAT-4-dependent glutamate signals from AWC stimulate the activity of AIY, and induce eventual migration to warmer side (red).

glutamate signals from AFD is larger than that of excitatory glutamate signals from AWC. Our study also showed that well-balanced glutamate signals from AFD and AWC could drive nearly normal responsiveness of AIY to temperature changes and eventual normal thermotaxis (Figures 3C and 4C). Taken together, glutamate signals from AFD and AWC are implied to be the critical factor for mediating the orchestration of major information in AFD and supportive information in AWC. In addition, our study demonstrated that GLC-3 receives EAT-4-dependent glutamate signals from AFD, although glutamate receptors that receive glutamate signals from AWC remained to be identified (Figures 5–7). The failure of finding excitatory glutamate receptors may possibly be caused by the difference in contribution between AFD and AWC for thermotaxis, thus reflecting the biased detection ability of thermotaxis defect towards AFD over AWC.

The RIA interneuron, known as one of the most pivotal interneurons in *C. elegans*, integrates signals processed in the thermotaxis neural circuit and emits outputs to downstream neurons (Figure 2C; Mori and Ohshima, 1995; Tanizawa *et al*, 2006). Given those previous reports, our work revealed that multiple transmissions including EAT-4-dependent glutamate from RIA are involved in communicating processed information in the circuit to downstream neurons, thereby generating ultimate thermotactic outputs (Figures 3 and 7D). Although there are no solid evidences as to which neurons downstream of RIA are main component neurons in the circuit, RIA is heavily connected with numerous presynapses to SMD or RMD head motor neurons that regulate turning behaviour (White *et al*, 1986; Gray *et al*, 2005). Considering that temperature regulates turn frequency and run duration (Zariwala *et al*, 2003), it is quite likely that SMD and RMD control turn frequency, depending on thermal information transmitted by RIA. We expect that inspection of glutamate transmission from RIA to SMD or to RMD, including identification of glutamate receptors functioning in SMD or RMD for thermotaxis, reveal the information processing that consequently generates a variety of thermotactic behavioural outputs.

Information processing in the simple circuit composed of AFD, AWC, and AIY neurons

Mori and Ohshima (1995) proposed the neural circuit for thermotaxis, in which AFD thermosensory neurons transmit excitatory signal to AIY interneurons. Consistent with this proposal, Clark *et al* (2006) showed using calcium imaging that AIY of animals lacking AFD did not respond to temperature changes. Given these results and our results on EAT-4, one can propose that the neural signals transmitted from AFD to AIY are of at least two kinds, EAT-4-dependent inhibitory signals and EAT-4-independent excitatory signals. In this study, we further showed that the thermotactic abnormality of *gcy-23 gcy-8 gcy-18* triple mutants with defective AFD function is considerably different from that of the *eat-4* mutants expressing EAT-4 in AWC and RIA, but not in AFD (*eat-4 (AWC +, RIA +)*; Figure 6A), and that AIY of *eat-4* mutants are hyper-responsive to temperature change than wild-type animals (Figure 4A and B), thereby undoubtedly implicating EAT-4-independent excitatory signals from AFD to AIY. Recent electrophysiological study showing that AFD responds to both cooling and warming (Ramot *et al*, 2008) is consistent with these results.

Our results also suggest that AWC transmit excitatory signals to AIY through EAT-4-dependent glutamatergic neurotransmission (Figure 4), although we previously reported that hyper-responsiveness of AWC to temperature change induced lower responsiveness of AIY (Kuhara *et al*, 2008). It is probable that AWC transmits EAT-4-independent inhibitory signals in addition to EAT-4-dependent excitatory glutamate signals to AIY, which is reminiscent of the regulation of behavioural response to odourants, in which AWC releases both glutamate and neuropeptide NLP-1 to postsynaptic AIA interneurons (Chalasani *et al*, 2010).

AWC senses odourants as well as temperature (Bargmann *et al*, 1993; Kuhara *et al*, 2008). How does *C. elegans* distinguish these qualitatively different signals within a sensory neuron? Similar to thermal signal, olfactory signal is transduced through G-protein signalling and cGMP-gated channels in AWC, and is further transmitted to AIY through EAT-4-dependent glutamatergic neurotransmission (Coburn and Bargmann, 1996; Roayaie *et al*, 1998; L'Etoile and Bargmann, 2000; Chalasani *et al*, 2007). Intriguingly, olfactory signal from AWC inhibits AIY on reception of glutamate signal by GLC-3/GluCl (Chalasani *et al*, 2007), whereas, as shown in this study, thermal signal from AWC stimulates AIY through putative glutamate receptors other than GLC-3/GluCl. Hence, our results demonstrated that segregation of different sensory signals, such as olfactory and thermosensory signals, is mediated through not only distinct signal transductions in a sensory neuron but also discrete neurotransmissions in downstream neural circuits.

We demonstrated one of the simplest neural circuits consisting of two different sensory neurons and a single postsynaptic interneuron, in which AFD and AWC sensory neurons use the same EAT-4/VGLUT-dependent glutamatergic neurotransmission to inhibit or stimulate the postsynaptic neuron AIY. The balance between inhibition and stimulation of the AIY activity significantly affected thermotactic behaviour. Strong EAT-4-dependent glutamatergic transmission from AFD enhanced the tendency for animals to migrate towards colder temperature than the cultivation temperature, whereas weak EAT-4-dependent transmission from AFD relative to AWC weakened the tendency to migrate to colder temperature and rather strengthened the tendency to migrate towards warmer temperature than the cultivation temperature. Thus, two synaptic transmissions encoding opposite information flows regulate neural activities to generate various behavioural outputs. Studies on synaptic transmission in the simple neural circuit consisting of AFD, AWC, and AIY should shed light onto information processing underlying vertebrate intertwined neural networks.

Materials and methods

Strains and genetics

eat-4 cDNA, *glr-3p::eat-4* cDNA, *ges-1p::NLS-GFP*] designated as *eat-4 (AWC+,RIA+)*, IK820 *eat-4 (AFD+, RIA+)* III; *glc-3(ok321)* V, IK822 *eat-4 (AWC+, RIA+)* III; *glc-3(ok321)* V, and many transgenic strains derived from them. *eat-4(nj2)* and *eat-4(nj6)* were isolated in genetic screens, as described by Okochi *et al* (2005) and mapped by multi-factor crosses and complementation tests with *eat-4(ky5)*. The isolated *eat-4* mutants were outcrossed to wild-type animals more than six times before the analyses.

Behavioural assays

The individual thermotaxis assay was performed as described by Mori and Ohshima (1995) and Mohri *et al* (2005). The population thermotaxis assay was performed as previously reported (Ito *et al*, 2006). Details of each assay are described in Supplementary data.

Molecular biology

The *eat-4* genomic fragment, including 2.4 or 5.5 kb of the promoter region and 2 kb of the downstream region, was amplified by PCR from N2 genome. The *full-length eat-4::gfp* translational fusion gene fragment, which was amplified by PCR from N2 genome and pPD95.75, contains a 5.5-kb fragment upstream of *eat-4* gene, *eat-4* gene (4.5 kb) including all exons and introns, *gfp* (0.9 kb), and 2-kb fragment downstream of *eat-4* gene.

For cell-specific rescue experiments, *cell-specific promoter::eat-4* cDNA construct and *cell-specific promoter::glc-3* cDNA construct were generated. *eat-4* cDNA was PCR amplified by using tagged primers from yk32h2 EST clone that contains *eat-4* cDNA lacking initial 7 bp, and was cloned into pPD49.26 to generate pNR8. *glc-3* cDNA was PCR amplified from yk1649c11 EST clone that contains full-length *glc-3* cDNA, and was cloned into pPD49.26 to generate pNR56. The resultant plasmids were confirmed to contain the intact cDNA by sequencing. All *cell-specific promoter::eat-4* cDNA plasmids and *cell-specific promoter::glc-3* cDNA plasmids were generated by inserting cell-specific promoter fragments into pNR8 or pNR56. All cell-specific promoter constructs were previously generated by PCR to contain only non-coding region. Before conducting the rescue experiments, expression patterns of *cell-specific promoter::gfp* constructs were verified by examining GFP fluorescence. Cell-specific promoters are 0.7 kb of *gcy-8p* for AFD, 2.3 kb of *odr-3p* for AWC, which also induces expression slightly in AWB, 0.8 kb of *ttx-3p* for AIY, 1.9 kb of *glr-3p* for RIA, 1.4 kb of *lin-11p* for AIZ, which also induces expression in ADF, AVJ, AVH, AVG, ADL, and RIC, 2.1 kb of *osm-6p* for sensory neurons, 5.3 kb of *glr-1p* for motor and command neurons, and 1.4 kb of *unc-14p* for all neurons.

For calcium imaging of AIY, *ttx-3p::yc3.60* construct was generated. Yellow cameleon 3.60 was amplified from YC3.60/pcDNA3 (Nagai *et al*, 2004) and cloned into pPD49.26 to generate pNR46. *ttx-3p* fragment was inserted into pNR46 to generate *ttx-3p::yc3.60* (pNR86). The resultant plasmid was confirmed to contain the intact *ttx-3p::yc3.60* by sequencing.

Transgenic animals

Germline transformation was performed by co-injecting experimental DNA (0.2–100 ng/μl) and an injection marker pKDK66 *ges-1p::NLS-GFP* (50 ng/μl) or pNAS88 *ges-1p::NLS TagRFP* (50 ng/μl) into the gonad (Mello *et al*, 1991). Multiple independent transgenic lines were established for each experimental DNA. For comparison of phenotypes on different genetic backgrounds, transgenic arrays were transferred by intercrossing.

In vivo calcium imaging and data analysis

In vivo calcium imaging was performed essentially according to previous reports with some modifications (Kimura *et al*, 2004;

Kuhara *et al*, 2008). After being cultivated at 20°C, well-fed animals expressing *ttx-3p::yc3.60* were glued onto a 1.5% agar pad on glass, immersed in M9 buffer, and covered by cover glass. The agar pad and M9 buffer were kept at the initial imaging temperature. Sample preparation was completed within 2 min. The sample was then placed onto a peltier-based thermocontroller (Tokai Hit, Japan) on the stage of an Olympus BX61WI at the initial imaging temperature for 2 min, and fluorescence was introduced into a Dual-View (Molecular Devices, USA) optics systems. Cyan fluorescent protein (CFP; F480) and yellow fluorescent protein (YFP; F535) images were simultaneously captured by an EM-CCD camera C9100-13 ImagEM (Hamamatsu Photonics). Images were taken with a 500 ms exposure time with 2×2 binning. The temperature on the agar pad was monitored by a thermometer system, DCM-20 (Tokai Hit and Hamamatsu Photonics). For each imaging experiment, fluorescence intensities of F535 and F480 were measured using MetaMorph imaging analysis system (Molecular Devices). As a computer regulates all the recorded images and the outcome of the analysis, any intention of a researcher should be excluded. Relative increases or decreases in the intracellular calcium concentration were measured as increases or decreases in the YFP/CFP fluorescence ratio of the cameleon protein (Ratio Change).

Statistics

All error bars in the figures indicate standard error of mean (s.e.m.). Results of behavioural experiments were treated as parametric data. The statistical analysis for all behavioural experiments was performed by one-way analysis of variance for multiple comparisons. Comparisons between each result were followed by *post hoc* Tukey–Kramer test, except for data sets including results of '0%'. Results of calcium imaging were treated as non-parametric data. The statistical analysis for all calcium imaging was performed by Steel–Dwass tests. A single asterisk (*), double asterisk (**), and non-significant (NS) in the figures indicate $P<0.05$, $P<0.01$, and $P>0.05$, respectively. Detailed statistical results in each figure are described in Supplementary data.

Supplementary data

Supplementary data are available at *The EMBO Journal* Online (http://www.embojournal.org).

Conflict of interest

The authors declare that they have no conflict of interest.

References

Bargmann C, Hartwieg E, Horvitz H (1993) Odorant-selective genes and neurons mediate olfaction in C. elegans. *Cell* **74:** 515–527

Bellocchio E, Reimer R, Fremeau RJ, Edwards R (2000) Uptake of glutamate into synaptic vesicles by an inorganic phosphate transporter. *Science* **289:** 957–960

Biron D, Wasserman S, Thomas J, Samuel A, Sengupta P (2008) An olfactory neuron responds stochastically to temperature and modulates Caenorhabditis elegans thermotactic behavior. *Proc Natl Acad Sci USA* **105:** 11002–11007

Brenner S (1974) The genetics of Caenorhabditis elegans. *Genetics* **77:** 71–94

Brockie P, Maricq A (2003) Ionotropic glutamate receptors in Caenorhabditis elegans. *Neurosignals* **12:** 108–125

Chalasani S, Chronis N, Tsunozaki M, Gray J, Ramot D, Goodman M, Bargmann C (2007) Dissecting a circuit for

olfactory behaviour in Caenorhabditis elegans. *Nature* **450:** 63–70

Chalasani S, Kato S, Albrecht D, Nakagawa T, Abbott L, Bargmann C (2010) Neuropeptide feedback modifies odor-evoked dynamics in Caenorhabditis elegans olfactory neurons. *Nat Neurosci* **13:** 615–621

Clark D, Biron D, Sengupta P, Samuel A (2006) The AFD sensory neurons encode multiple functions underlying thermotactic behavior in Caenorhabditis elegans. *J Neurosci* **26:** 7444–7451

Clark D, Gabel C, Lee T, Samuel A (2007) Short-term adaptation and temporal processing in the cryophilic response of Caenorhabditis elegans. *J Neurophysiol* **97:** 1903–1910

Coburn C, Bargmann C (1996) A putative cyclic nucleotide-gated channel is required for sensory development and function in C. elegans. *Neuron* **17:** 695–706

de Bono M, Maricq A (2005) Neuronal substrates of complex behaviors in C. elegans. *Annu Rev Neurosci* **28:** 451–501

Dent J, Davis M, Avery L (1997) avr-15 encodes a chloride channel subunit that mediates inhibitory glutamatergic neurotransmission and ivermectin sensitivity in Caenorhabditis elegans. *EMBO J* **16:** 5867–5879

Di Maio V (2008) Regulation of information passing by synaptic transmission: a short review. *Brain Res* **1225:** 26–38

Dillon J, Hopper N, Holden-Dye L, O'Connor V (2006) Molecular characterization of the metabotropic glutamate receptor family in Caenorhabditis elegans. *Biochem Soc Trans* **34:** 942–948

Gomez M, De Castro E, Guarin E, Sasakura H, Kuhara A, Mori I, Bartfai T, Bargmann C, Nef P (2001) Ca2+ signaling via the neuronal calcium sensor-1 regulates associative learning and memory in C. elegans. *Neuron* **30:** 241–248

Gray J, Hill J, Bargmann C (2005) A circuit for navigation in Caenorhabditis elegans. *Proc Natl Acad Sci USA* **102:** 3184–3191

Hall D, Hedgecock E (1991) Kinesin-related gene unc-104 is required for axonal transport of synaptic vesicles in C. elegans. *Cell* **65:** 837–847

Hedgecock E, Russell R (1975) Normal and mutant thermotaxis in the nematode Caenorhabditis elegans. *Proc Natl Acad Sci USA* **72:** 4061–4065

Hills T, Brockie P, Maricq A (2004) Dopamine and glutamate control area-restricted search behavior in Caenorhabditis elegans. *J Neurosci* **24:** 1217–1225

Hobert O, Mori I, Yamashita Y, Honda H, Ohshima Y, Liu Y, Ruvkun G (1997) Regulation of interneuron function in the C. elegans thermoregulatory pathway by the ttx-3 LIM homeobox gene. *Neuron* **19:** 345–357

Horoszok L, Raymond V, Sattelle D, Wolstenholme A (2001) GLC-3: a novel fipronil and BIDN-sensitive, but picrotoxinin-insensitive, L-glutamate-gated chloride channel subunit from Caenorhabditis elegans. *Br J Pharmacol* **132:** 1247–1254

Inada H, Ito H, Satterlee J, Sengupta P, Matsumoto K, Mori I (2006) Identification of guanylyl cyclases that function in thermosensory neurons of Caenorhabditis elegans. *Genetics* **172:** 2239–2252

Ito H, Inada H, Mori I (2006) Quantitative analysis of thermotaxis in the nematode Caenorhabditis elegans. *J Neurosci Methods* **154:** 45–52

Kerr R, Lev-Ram V, Baird G, Vincent P, Tsien R, Schafer W (2000) Optical imaging of calcium transients in neurons and pharyngeal muscle of C. elegans. *Neuron* **26:** 583–594

Kimura K, Miyawaki A, Matsumoto K, Mori I (2004) The C. elegans thermosensory neuron AFD responds to warming. *Curr Biol* **14:** 1291–1295

Komatsu H, Mori I, Rhee J, Akaike N, Ohshima Y (1996) Mutations in a cyclic nucleotide-gated channel lead to abnormal thermosensation and chemosensation in C. elegans. *Neuron* **17:** 707–718

Kuhara A, Okumura M, Kimata T, Tanizawa Y, Takano R, Kimura K, Inada H, Matsumoto K, Mori I (2008) Temperature sensing by an olfactory neuron in a circuit controlling behavior of C. elegans. *Science* **320:** 803–807

L'Etoile N, Bargmann C (2000) Olfaction and odor discrimination are mediated by the C. elegans guanylyl cyclase ODR-1. *Neuron* **25:** 575–586

Lee R, Sawin E, Chalfie M, Horvitz H, Avery L (1999) EAT-4, a homolog of a mammalian sodium-dependent inorganic phosphate cotransporter, is necessary for glutamatergic neurotransmission in Caenorhabditis elegans. *J Neurosci* **19:** 159–167

Mello C, Kramer J, Stinchcomb D, Ambros V (1991) Efficient gene transfer in C. elegans: extrachromosomal maintenance and integration of transforming sequences. *EMBO J* **10:** 3959–3970

Miyawaki A, Llopis J, Heim R, McCaffery J, Adams J, Ikura M, Tsien R (1997) Fluorescent indicators for Ca2+ based on green fluorescent proteins and calmodulin. *Nature* **388:** 882–887

Mohri A, Kodama E, Kimura K, Koike M, Mizuno T, Mori I (2005) Genetic control of temperature preference in the nematode Caenorhabditis elegans. *Genetics* **169:** 1437–1450

Mori I, Ohshima Y (1995) Neural regulation of thermotaxis in Caenorhabditis elegans. *Nature* **376:** 344–348

Nagai T, Yamada S, Tominaga T, Ichikawa M, Miyawaki A (2004) Expanded dynamic range of fluorescent indicators for Ca(2+) by circularly permuted yellow fluorescent proteins. *Proc Natl Acad Sci USA* **101:** 10554–10559

Ni B, Rosteck PJ, Nadi N, Paul S (1994) Cloning and expression of a cDNA encoding a brain-specific Na(+)-dependent inorganic phosphate cotransporter. *Proc Natl Acad Sci USA* **91:** 5607–5611

Okochi Y, Kimura K, Ohta A, Mori I (2005) Diverse regulation of sensory signaling by C. elegans nPKC-epsilon/eta TTX-4. *EMBO J* **24:** 2127–2137

Otsuka A, Jeyaprakash A, García-Añoveros J, Tang L, Fisk G, Hartshorne T, Franco R, Born T (1991) The C. elegans unc-104 gene encodes a putative kinesin heavy chain-like protein. *Neuron* **6:** 113–122

Ramot D, MacInnis B, Goodman M (2008) Bidirectional temperature-sensing by a single thermosensory neuron in C. elegans. *Nat Neurosci* **11:** 908–915

Rankin C, Wicks S (2000) Mutations of the Caenorhabditis elegans brain-specific inorganic phosphate transporter eat-4 affect habituation of the tap-withdrawal response without affecting the response itself. *J Neurosci* **20:** 4337–4344

Roayaie K, Crump J, Sagasti A, Bargmann C (1998) The G alpha protein ODR-3 mediates olfactory and nociceptive function and controls cilium morphogenesis in C. elegans olfactory neurons. *Neuron* **20:** 55–67

Ségalat L, Elkes D, Kaplan J (1995) Modulation of serotonin-controlled behaviors by Go in Caenorhabditis elegans. *Science* **267:** 1648–1651

Sulston J, Horvitz H (1977) Post-embryonic cell lineages of the nematode, Caenorhabditis elegans. *Dev Biol* **56:** 110–156

Sulston J, Schierenberg E, White J, Thomson J (1983) The embryonic cell lineage of the nematode Caenorhabditis elegans. *Dev Biol* **100:** 64–119

Takamori S, Rhee J, Rosenmund C, Jahn R (2000) Identification of a vesicular glutamate transporter that defines a glutamatergic phenotype in neurons. *Nature* **407:** 189–194

Tanizawa Y, Kuhara A, Inada H, Kodama E, Mizuno T, Mori I (2006) Inositol monophosphatase regulates localization of synaptic components and behavior in the mature nervous system of C. elegans. *Genes Dev* **20:** 3296–3310

Wenick A, Hobert O (2004) Genomic cis-regulatory architecture and trans-acting regulators of a single interneuron-specific gene battery in C. elegans. *Dev Cell* **6:** 757–770

White J, Southgate E, Thomson J, Brenner S (1986) The Structure of the Nervous System of the Nematode Caenorhabditis elegans. *Phil Trans R Soc London Series B Biol Sci* **314:** 1–340

Yates D, Portillo V, Wolstenholme A (2003) The avermectin receptors of Haemonchus contortus and Caenorhabditis elegans. *Int J Parasitol* **33:** 1183–1193

Zariwala H, Miller A, Faumont S, Lockery S (2003) Step response analysis of thermotaxis in Caenorhabditis elegans. *J Neurosci* **23:** 4369–4377